Observations of Transient Linear Organization and Nonlinear Scale Interactions in Lake-Effect Clouds. Part II: Nonlinear Scale Interactions

NATASHA L. MILES AND JOHANNES VERLINDE

Department of Meteorology, The Pennsylvania State University, University Park, Pennsylvania

(Manuscript received 2 September 2003, in final form 10 August 2004)

ABSTRACT

Linearly organized convection and associated horizontal roll vortices occasionally occur in atmospheric conditions in which theory predicts only cellular organization. One possible contributor to the occurrence of rolls in such conditions is nonlinear interactions between different scales of motion. In the winter of 1997/98, the Lake-Induced Convection Experiment (Lake-ICE) was conducted in part to investigate scale interactions in linearly organized convection. As discussed in Part I of this series, transient linear organization was observed during a wintertime lake-effect event during Lake-ICE. In Part II two-part nonlinear scale interactions and their possible role in the occurrence of linear organization in an unfavorable environment are investigated. Turbulence-scale vertical velocity variance peaks were consistently observed during roll strengthening and decay, suggesting a link between the scales. Composites of the nonlinear interaction terms in the roll-scale vertical turbulent kinetic energy (TKE) budget revealed that nonlinear interactions between the roll and turbulence scales were large compared to the observed change in roll-scale TKE, but do not coincide in time.

1. Introduction

Only a few studies have documented transitions between linear and nonlinear organization (Braham 1986; Weckwerth et al. 1999; Kristovich et al. 1999). In this first part of this series (Miles and Verlinde 2005, hereafter referred to as Part I) we observed transient linear organization using vertical velocities derived from vertically pointing cloud radar data collected during the Lake-Induced Convection Experiment (Lake-ICE). We showed that the transitions between organized and random convection occurred in an environment generally unfavorable for linearly organized convection. Furthermore, we found no correlation of atmospheric conditions (boundary layer mean shear, low-level shear, shear curvature, temperature, buoyancy flux, and stability parameter) with the observed organization. In this paper, we investigate another possible cause: nonlinear interactions between large (roll) and small (turbulence) scales.

Past studies have indicated that, in certain circumstances, different scales of motion can interact with each other. LeMone (1976) found that roll circulations acted to concentrate turbulence-producing eddies in the updraft regions, thus affecting the turbulence kinetic energy. In partly cloudy conditions, LeMone and Pennell (1976) found that subcloud layer fluxes were enhanced beneath cloud streets and 40-km-scale cloud patches, indicating a connection between these structures and the subcloud layer eddies. With an airborne downward-looking lidar and aircraft data, Melfi et al. (1985) and Atlas et al. (1986) found evidence of interactive convective cells and rolls, as well as structures with scales of 100–300 m. Reinking et al. (1981) and Rabin et al. (1982) utilized dual-Doppler and aircraft data to observe rolls and more energetic larger-scale (i.e., >1 km) turbulence in cloudless convective layers. Nicholls (1978) found evidence consistent with convective elements organized into preferred areas roughly aligned with the mean wind.

Nonlinear interactions may contribute to mode switching in marginal cases such as the present one. Several studies have suggested that nonlinear interactions contribute to changes in the convective scale. For example, Chang and Shirer (1984), in their modeling study of mesoscale cellular convection, suggested that nonlinearity can produce energy transfer between different scales of motion. Mourad and Brown (1990) proposed a theory that the coexistence of scales of motion on the order of the boundary layer depth with scales of motion several times this depth are generated by nonlinear interaction among unstable waves. Numerical

Corresponding author address: Dr. Natasha L. Miles, Dept. of Meteorology, College of Earth and Mineral Sciences, The Pennsylvania State University, 503 Walker Building, University Park, PA 16802.
E-mail: nmiles@met.psu.edu

simulations in two dimensions by Rothermel and Agee (1986) suggested that upscale transfer might be responsible for the large aspect ratios (i.e., ratio of width to height of boundary layer structures) typically observed in mesoscale cellular convection. In a similar two-dimensional study, however, the maximum aspect ratio did not increase beyond three (Sykes and Henn 1988). Such two-dimensional studies must be viewed with caution because there is no mechanism for downscale energy transfer (from the energy-containing scales to the dissipative scales) in two-dimensional turbulence (e.g., Glendening 1996).

Other possibilities for changes in convective organization can be considered by examining terms in the turbulent kinetic energy (TKE) budget. Examining specifically roll-scale TKE using tower and aircraft data, LeMone (1973) found both mean shear and buoyancy to be important production terms. Brümmer (1985) and Hein and Brown (1988) evaluated the roll-scale TKE budget, treating the sum of the roll-scale pressure transport, vertical transport, and interaction between rolls and turbulence as a residual. Brümmer (1985) found rolls driven by mean shear and, on different days, rolls driven by buoyancy. In the case investigated by Hein and Brown (1988), both buoyancy and cross-wind shear were important terms. In a large-eddy simulation (LES) study of roll vortices with strong wind shear and moderate surface buoyancy flux, Glendening (2000) found that buoyancy converted into horizontal energy by pressure forcing was the major source of roll energy, not cross-roll shear. In the upper half of the boundary layer, buoyancy, vertical transport, and nonlinear interactions all contributed significantly to the roll-scale vertical TKE budget, while in the lower half of the boundary layer buoyancy dominated the production terms, and both vertical transport and nonlinear interaction terms were losses to roll-scale TKE.

Previous work has suggested that latent heating can be important to convection in general, and to the convective organization in particular. Two-dimensional cloud-resolving model studies by Olsson and Harrington (2000) and Harrington and Olsson (2001) suggested that boundary layer dynamics is influenced by cloud microphysical processes and, hence, latent heating. Olsson and Harrington (2000) concluded that simulated clouds containing both liquid and ice cloud particles produced more shallow boundary layers with less vigorous turbulence than those containing only ice cloud particles. Ensuing studies by Harrington and Olsson (2001) found the reduced turbulent intensity to be caused by precipitation. In addition, TKE profiles indicated that latent heating contributes substantially to the TKE budget (Olsson and Harrington 2000). In a comparison of LES model runs with and without the effects of condensation and evaporation, Rao and Agee (1996) showed that latent heating increased the vertical velocity variance in the upper part of the cloud, and evaporative cooling decreased the variance in the subcloud layer.

The results of an LES study by Chlond (1992) suggested that latent heating can intensify roll circulations once rolls have developed. Brümmer (1997, 1999) studied arctic cold-air outbreaks during which air flows from an ice-covered region to open water. In this type of situation, rolls often form closest to the ice edge and transition into cells farther downstream. Brümmer (1997) found latent heating more important to the heat budget in cellular convection regions than in roll convection regions. Brümmer (1999) found greater values of latent heating in cellular convections regions than in roll convection regions. He then hypothesized that condensation is important in the transition from linear convection to cellular convection in arctic cold-air outbreaks. Similarly, Kristovich et al. (1999) observed a tendency for cellular convection, and increased vertical motions, when clouds were present. Latent heating has also been shown to play a role in increased roll aspect ratios (e.g., Sykes et al. 1988; Hartmann et al. 1997) and increased cell aspect ratios (Müller and Chlond 1996).

As a whole, these studies suggest that interactions between different scales of motion may impact the formation and maintenance of rolls. We thus investigate the role of nonlinear scale interactions in the transient linear organization observed during Lake-ICE on the downwind shore of Lake Michigan (Part I).

2. Transitions between linear and cellular convection

To take a closer look at the possible contributors to the mode switching, we investigate the cloud radar observations in greater detail. Building on results from and using the three scales (turbulence, cell, and roll) as defined by Part I, in Fig. 1 we plot the roll-scale vertical velocity w^r, superimposing the wavelet amplitude integrated between the roll period range (39.3–55.6 min). There are three cycles apparent in the w^r trace, corresponding to the three peaks in the roll-scale range from wavelet analysis. There is also a hint of another peak between the second and third cycles but its power is comparatively much lower. We partition each cycle into 10 stages, defined such that roll updrafts occur during odd-numbered stages and roll downdrafts occur during even-numbered stages. Stage 0 is the stage prior to the beginning of roll growth, stage 1 is prior to the maximum roll intensity, and stage 5 is what we call a mature-roll stage in which there is large roll-scale variance and identifiable rolls. For each of the cycles, excluding the last, the rolls have decayed by stage 8. Stage 9 is defined as the period between the end of stage 8 and the beginning of stage 0 in the next cycle. This choice, while having the disadvantage of stage 9 being defined differently from the other stages, has the advantage of continuously defined stages. The length of stage 9 in the

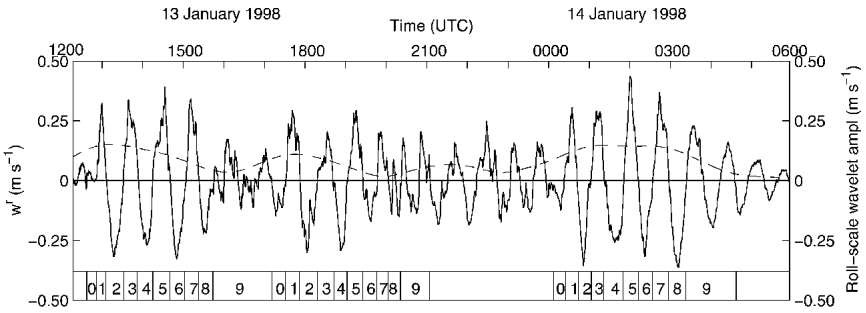

FIG. 1. Roll-scale vertical velocity at a height of 720 m (solid line) and roll-scale wavelet amplitude, also at 720 m (dashed line). The stages of the roll life cycle are indicated near the bottom of the figure.

third cycle was taken to be the average of its length in the first and second cycles.

The choice of stages is a compromise between accommodating the roll updraft and downdraft structure, maintaining an equal number of stages, and considering the roll-scale wavelet amplitude. For example, since the last cycle continues longer than the first two, its stages 7 and 8 could have been defined as the roll updraft and downdraft following the stages 7 and 8 shown in Fig. 1. This definition would, however, result in discontinuously defined stages. Alternatively, additional stages could have been added for the last cycle. The composite of the additional stages would have, however, then included data only from that cycle, and thus would not be particularly useful. The perhaps more serious problem is that we have only three cycles over which to composite. This is a fundamental problem due to the duration of the roll life cycle—about 5 h—and the duration of the lake-effect event—about 18 h.

a. Variance profiles

Before considering the details of the interactions between scales, we first focus on the overall structure of the vertical velocity turbulence statistics during the analysis period. We use a Reynolds decomposition algorithm with piecewise maximally overlapping windows (Moyer and Young 1994; Young et al. 2000) to compute the variance of the turbulence-scale vertical velocity. The window length is chosen such that the ratio between window length and the depth of the boundary layer is 12:1. This ratio results in 20%–25% accuracy for measured variances (Lenschow and Stankov 1986). With average in-cloud wind speed of 7.5 m s^{-1} and average downwind boundary layer depth (z_i) of 890 m, the window length necessary to achieve this ratio is 23.8 min.

The derived variance profiles are shown in Fig. 2, where we show only every twentieth profile for the sake of clarity. Points above cloud top, as determined using the cloud mask, were excluded from the calculations, and windows with greater than 60% excluded points were not plotted. Profiles separated by fewer than four other profiles have windows that overlap. In this figure we seek to highlight the shape tendencies rather than the magnitude of the variance. Figure 2 reveals several periods of well-defined midcloud variance peaks, the most prominent of which begin at the following approximate times: 1247, 1507, 1717, 2017, 2127, 2327, 0017, and 0137 UTC. Each of the three stage 0–1 periods, as well as each of the three stage 7–8 periods, have profiles with more or less well-defined midcloud peaks. Although there are a few additional periods of well-defined midcloud peaks, for the most part the profiles during other times are either linearly decreasing with height or not dependent on height.

For clear and fair-weather cumulus conditions, numerous models (Sommeria and LeMone 1978; Deardorff 1980; Moeng 1984) and observational studies (e.g., Hildebrand and Ackerman 1984; Young 1988) revealed a single mid-boundary-layer vertical velocity variance peak, typically at heights between 0.3 and 0.5 z_i. In cases of active cloud formation or significant liquid water paths, however, a secondary, in-cloud peak is frequently found (Sommeria and LeMone 1978; Deardorff 1980; Nicholls 1984; Frisch et al. 1995; Rao and Agee 1996; Lappen and Randall 2001). Several mechanisms for the production of these secondary, in-cloud peaks have been proposed: evaporative cooling of descending entraining air near cloud top (Deardorff 1980), longwave radiative cooling at cloud top (Frisch et al. 1995), and latent heating (Rao and Agee 1996). The presence of ice may also be important, as Harrington and Olsson (2001) found reduced variance in simulations including mixed-phase precipitation compared to those including only liquid precipitation. It is the in-cloud peak, or lack thereof, that can be seen in the cloud radar data.

The transient nature of the secondary variance peaks and their proximity to mode-switching times suggest a possible relationship between the turbulence activity and mode switching. To better quantify the relative strengths of the midcloud variance, we define a "peakedness parameter." First, the second-degree polynomial that best fits the data, in a least squares sense, is

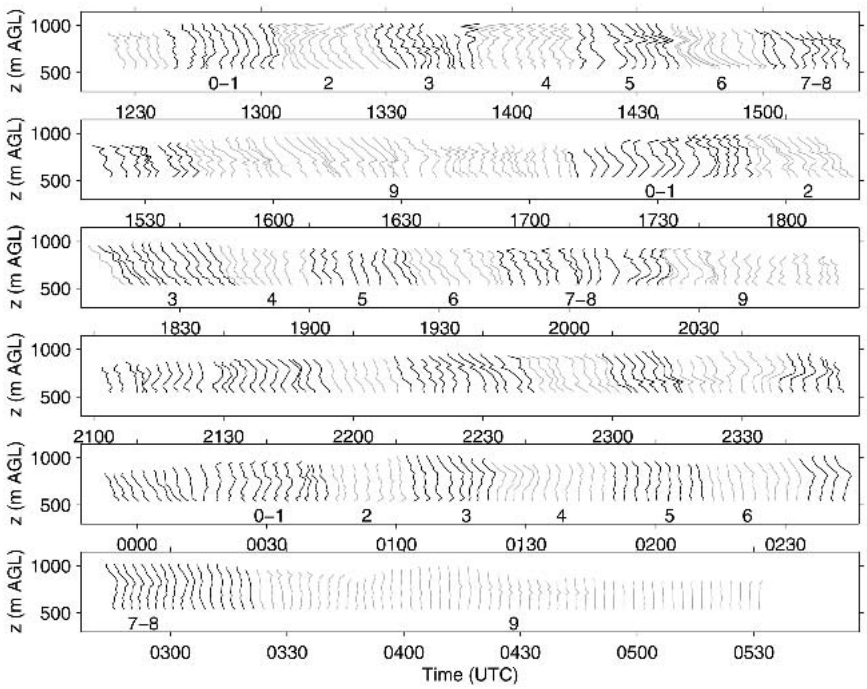

FIG. 2. Turbulence-scale vertical velocity variance profiles. Alternate stages are presented as light/dark lines and are identified according to stage number below the profiles.

determined for each of the variance profiles. A profile without an extremum between the endpoints is assigned a peakedness parameter of zero. If the fitted data do have an extremum between the endpoints, the peakedness parameter is calculated as the difference between the extremum and the average of the endpoints, divided by the mean of the profile. A positive value for the peakedness parameter indicates a profile with a maximum between the endpoints, and a negative value indicates a profile with a minimum between the endpoints.

The peakedness parameter for the turbulence-scale variance throughout the time series, shown in Fig. 3, confirms the visual impression of peakedness in Fig. 2. In summary, the only stages that are consistent across all three cycles are 0–1 and 7–8, which have positive peakedness, meaning that these stages persistently have in-cloud vertical velocity variance maxima. Peakedness for the other stages varies from cycle to cycle.

b. Composite of roll life cycle

Compositing is a method used by numerous authors (e.g., LeMone 1973; Brümmer 1997; Young et al. 2000) to isolate systematic from random variations. We now composite, or average, over three cycles of roll growth and roll decay. Although there is a hint of another cycle

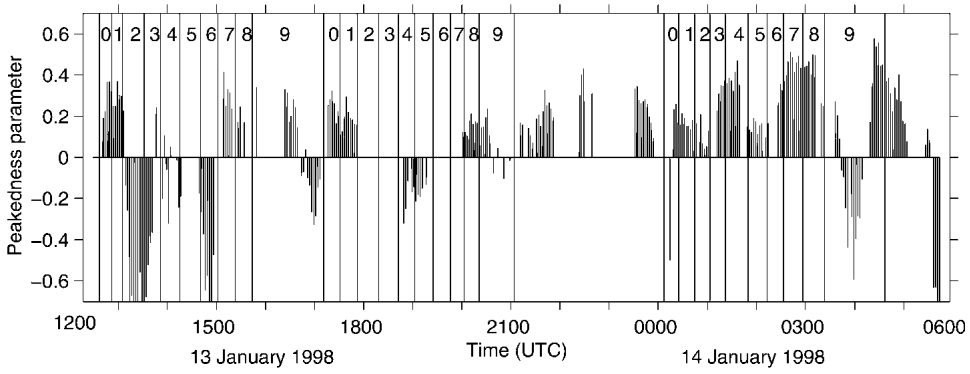

FIG. 3. Peakedness parameter for the profiles shown in Fig. 2. The vertical lines separate the various stages of the roll life cycle.

between the second and third cycles (Fig. 1), it is comparatively weak and is therefore excluded from the presented results.

To form composite variance profiles for each of the different scales, we first calculate the variance of the filtered vertical velocities in each stage of each cycle at each height. These variance profiles are then mapped onto a cloud-normalized height scale ranging from cloud base ($h = 0$) to cloud top ($h = 1$). The results for each of the 10 stages are then averaged over the three cycles. The normalization factor used is the time average of the variance in all 10 stages for each scale, also averaged over height from cloud base to cloud top. The normalized integrated variance profiles for stages 1 (during roll formation) and 5 (mature rolls) are shown in Fig. 4 for each of the three scales: turbulence, cell, and roll. We are primarily interested in the shape of the profiles rather than the magnitude. The standard deviation of profiles with the similar shapes but different magnitudes does not reveal the similarity between the shapes of the profiles. Thus, in calculating the standard deviations, we first force the three composited profiles for each stage to the same mean. This procedure does not affect the composite profiles, only the standard deviation. Since we composite over only three cycles, the standard deviation is highly dependent on each data point.

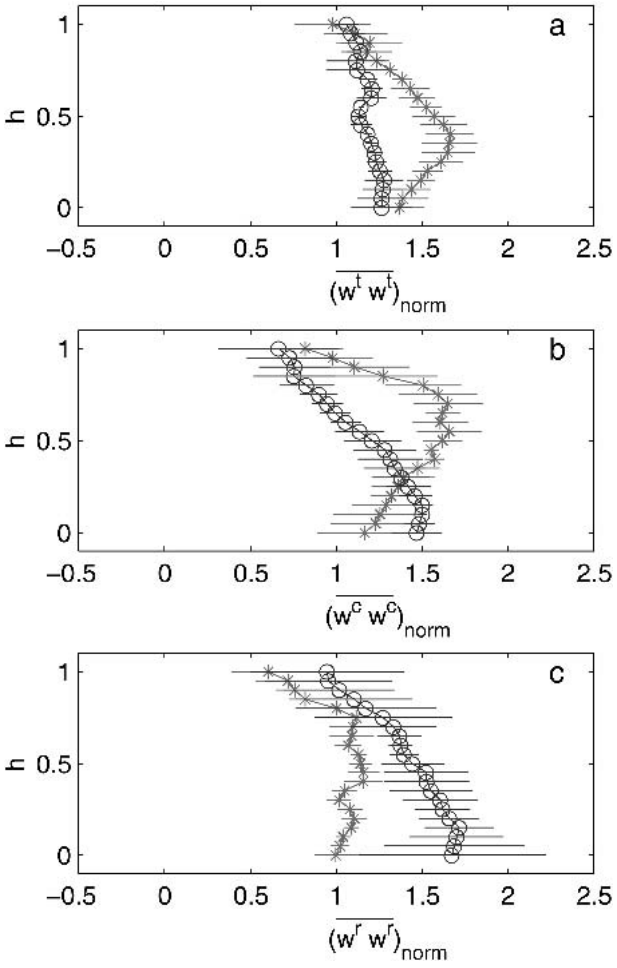

FIG. 4. Normalized variance profiles composited over three roll life cycles for each of three scales: (a) turbulence, (b) cell, and (c) roll. Profiles during stage 1, prior to maximum roll intensity, are indicated by stars. Profiles during stage 5, a mature-roll stage, are indicated by open circles. The cloud normalized height h is defined to be zero at cloud base and one at cloud top.

In Fig. 4a, the turbulence-scale variance profile in stage 1 shows a midcloud peak, as expected from the results shown in Fig. 2. The equivalent profile during a mature-roll stage is approximately constant with height. In Fig. 4c, roughly opposite behavior occurs—that is, the stage-5 roll-scale variance is high and decreases with height—whereas the stage-1 roll-scale variance is lower and approximately constant with height. The behavior of the cell-scale variance profiles (Fig. 4b) is similar to that of the turbulence-scale profiles, with two exceptions. The cell-scale variance profiles at stages 1 and 5 cross in the lower part of the cloud layer, whereas the turbulence-scale profiles do not. The peak in the stage-1 cell-scale variance profile occurs at a level higher in the cloud than that of the stage-1 turbulence-scale variance profile. This trend may be a consequence of turbulence-scale eddies merging with height to form cells during stage 1.

To focus on the variability of the 10 stages, the calculated variances are averaged over height (based on the cloud base and cloud top of each stage of each cycle) and plotted as a function of stage, shown in Fig. 5a, for the turbulence- and roll-scale variance. The cell-scale variance is not shown since it is strongly correlated to the turbulence-scale variance. As in Fig. 4, the results are normalized by the time average of the variance in all 10 stages for each scale, also averaged over height from cloud base to cloud top. The normalization factor for the roll-scale variance ($0.026\ m^2\ s^{-2}$) is about 4% of that of the turbulence-scale variance.

In Fig. 5a, the overall trend of the roll life cycle is very little roll-scale variance at stage 0, maximum variance during the midrange stages, and by stage 8 the variance has decreased to below the mean. The turbulence-scale eddies are more energetic during roll updraft (odd numbered) stages (Fig. 5a), although the difference is not large compared to the error bars. The concentration of plumes into roll updraft areas favorable for growth is in agreement with the results of previous authors (e.g., LeMone 1976; Sommeria and LeMone 1978). The turbulence-scale variance is, in general, high when the roll-scale variance is low, and low when the roll-scale variance is high. The turbulence-scale variance peaks at stage 1, just prior to a peak in the roll-scale variance. The turbulence-scale variance then falls off, has a lesser peak at stage 5, and begins to increase over the last three stages. The overall trend is more easily apparent in Fig. 5b, in which successive downdraft and updraft stages are grouped to-

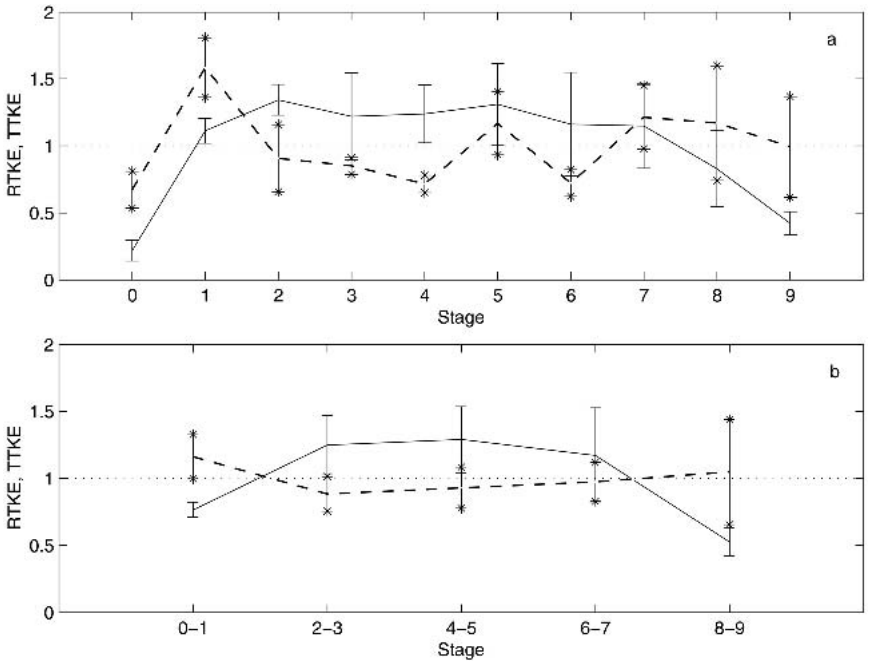

FIG. 5. (a) Composites of normalized integrated roll-scale variance (solid line) and turbulence-scale variance (dashed line) as a function of stage in roll life cycle. (b) Same as (a), except stages 0–1, 2–3, 4–5, 6–7, and 8–9 are grouped together. The error bars indicate the standard deviation of the three cycles. The endpoints of the error bars for the turbulence-scale variance are marked with stars, and those of the roll-scale variance are marked with small horizontal bars.

gether. The results shown in Figs. 5a and 5b suggest a possible exchange of energy between turbulence and roll scales, particularly in the early stages of roll development (stages 0–2) when the turbulence-scale variance peak immediately precedes a prominent peak in the roll-scale variance.

3. Scale interactions

a. Nonlinear interaction and vertical transport terms

We now consider the possible contribution of scale interactions to the observed mode switches by investigating the terms in the roll-scale turbulent kinetic energy budget. We follow Wyngaard (2002) in his derivation of the roll-scale turbulent kinetic energy equation, although we differ in that we separate the fluctuating vertical velocity into roll- and turbulence-scale parts, denoted by w^r and w^t, respectively. The vertical component of this equation as can then be written as

$$\frac{\partial\left(\frac{1}{2}\overline{w^r w^r}\right)}{\partial t} + \mathrm{ADV} = \mathrm{MS} + B + \mathrm{PT} + C + (\mathrm{ITTT})_r, \tag{1}$$

where the terms are the local time rate of change of the roll-scale vertical TKE, advection (ADV), mean shear production (MS), buoyancy production (B), pressure transport (PT), Coriolis intercomponent transfer (C), and interscale transfer and turbulent transport [$(\mathrm{ITTT})_r$]. We focus on the interscale transfer and turbulent transport term. We do not have the information necessary to evaluate the other terms specifically, although we did show in Part I that neither shear nor buoyancy appeared to incite changes in mesoscale organization.

According to Wyngaard (2002), the interscale transfer terms have the form of a stress tensor contracted with a strain-rate tensor. This results in five terms in the roll-scale vertical TKE equation that contain only vertical velocity terms:

$$(\mathrm{ITTT})_r = \underbrace{-\frac{1}{2}\frac{\partial\overline{w^r w^r w^r}}{\partial z}}_{\mathrm{RVT}} - \frac{\partial\overline{w^r w^r w^t}}{\partial z} + \overline{w^r w^r}\frac{\partial w^t}{\partial z}$$

$$\underbrace{-\frac{\partial\overline{w^r w^t w^t}}{\partial z}}_{\mathrm{SW}} + \underbrace{\overline{w^t w^t}\frac{\partial w^r}{\partial z}}_{\mathrm{RSS}}. \tag{2}$$

The terms in Eq. (2) are, in order, vertical transport of roll-scale vertical component of TKE by the rolls (RVT), vertical transport of roll-scale vertical compo-

nent of TKE by the turbulence, turbulence shear stress interscale transfer, vertical transport of turbulence-scale vertical component of TKE by the rolls, and roll shear stress interscale transfer. Following Glendening (2000, hereafter referred to as Glendening), we call the fourth term stress work (SW) and the last term roll shear stress (RSS). We take w^r to be the roll-scale vertical velocity, and w^t to include the vertical velocity of the turbulence scale, the cell scale, and scales between the roll scale and the cell scale. Comparable analysis with w^t instead being only turbulence-scale vertical velocity yielded qualitatively similar results, since the majority of the variance is turbulence scale.

Composites of the terms in Eq. (2), integrated over the cloud layer, are shown in Fig. 6. The second and third terms in Eq. (2) are negligible. The small magnitude of these terms is partially a consequence of the magnitude of the roll-scale TKE being only 4% of that of the turbulence-scale TKE. The roll-scale vertical transport is very small compared to the RSS and SW, but is slightly positive during roll updraft (odd numbered) stages and slightly negative during roll downdraft (even numbered) stages. The stress work and roll shear stress terms dominate the net effect of the interscale transfer and turbulent transport. The stress work term is generally positive during roll updrafts and negative during roll downdrafts, but the magnitude is larger during the updraft stages, indicating that, overall, it is a gain in the roll-scale TKE equation. When the stress work term is positive, turbulence-scale stress is transported into the cloud layer by the rolls and "consumed" by the roll-scale TKE. The roll shear stress interscale transfer term counteracts the stress work term, being negative in roll updraft stages and positive in roll downdraft stages. The one exception is stage 6 in which both terms are negative. The negative roll shear stress terms indicate net downscale transfer from the roll scale to the turbulence scales, whereas positive values indicate net upscale transfer.

Vertical profiles of the two dominant turbulent transport and interscale transfer terms, roll shear stress and stress work, and their sum (all normalized by w_*^3/z_i) are plotted in Fig. 7, for stage 5, a mature-roll stage. The roll shear stress is negative throughout most of the cloud, but is positive near cloud base. The sign of the stress work term is opposite that of the roll shear stress, but its magnitude is generally larger; thus the sum of the two terms (hereafter, net nonlinear interaction) is positive throughout the cloud layer.

We compare our results for the vertical transport and nonlinear interaction terms with those of a modeling study of Glendening and an observational study by LeMone (1976). Glendening analyzed results from a large-eddy simulation with domain size of 24.6 km $\times$ 18.4 km in the horizontal plane, and 1.0 km in the vertical direction. The number of grid points was quite large: 384 $\times$ 288 $\times$ 32. The simulation was highly sheared, with the value of u_*/w_* being 0.54 at the analyzed time. In Glendening's analysis, the statistics were averaged along lines parallel to the roll direction within a rectangular subdomain centered on a roll updraft. Using aircraft data collected in Colorado and the Lake Michigan area, LeMone (1976) averaged data from several rolls to form composite rolls for each of three cases. This process approximates averaging in the along-roll direction, as in Glendening, if the rolls are uniform and if the length of the rolls is much larger than their width. In the present case we also composite, but we are interested in changes that occur as the organization switches between linear and cellular, over what we call the "roll life cycle." We thus calculate the composite of the roll life cycle, which emcompasses several rolls. A consequence of this difference is that w^r is not constant over our averaging interval, which is a "stage," as previously defined.

A few cautionary remarks are in order for the comparisons with Glendening's results. A fundamental difference between the present results and those of Glendening is that we separate the different contributions to the vertical velocity variance in frequency space, whereas Glendening's separation was in physical space. He decomposed the total TKE into lineal (Ltke) and nonlineal (NLtke) parts, where the lineal part is the average along a line oriented parallel to the roll direc-

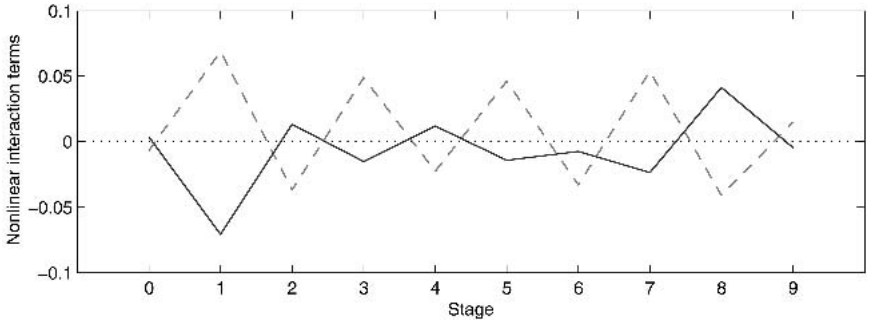

FIG. 6. Composite of vertical transport and interscale transfer terms in the roll-scale vertical TKE budget, averaged over the cloud depth, as a function of stage. Solid line: RSS; dashed line: SW. The remaining three terms are so nearly zero that they are not plotted.

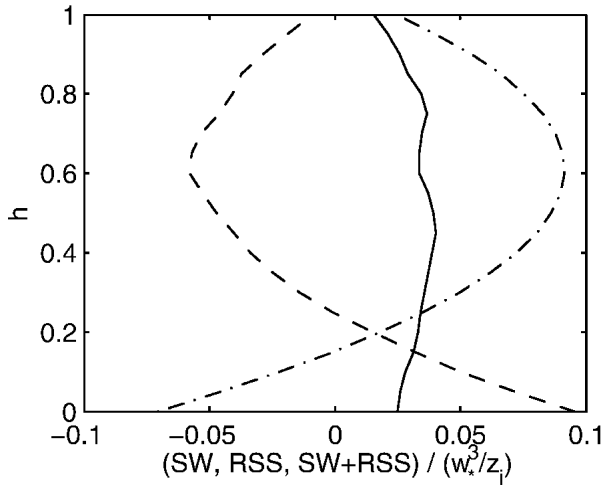

FIG. 7. Composited vertical profiles of normalized stress work (dot–dash line), roll shear stress (dashed line), and their sum (solid line) for stage 5, when the rolls are well developed. The cloud normalized height h is defined to be zero at cloud base and one at cloud top.

tion and the nonlineal part is the deviation from that average. The lineal TKE was then further decomposed into roll TKE (Rtke), containing cross-roll (x direction) and vertical components, and along-roll (y direction) lineal TKE (Vtke). The total TKE includes only resolved-scale TKE, not subgrid-scale TKE. Since the resolution of the LES was 32 m horizontally and 64 m vertically, the smallest-size eddies resolved are on the order of 100 m, near the minimum scale detectable by the cloud radar in this study. Because the vertically pointing cloud radar measures only vertical velocity, we do not have data for the along-axis lineal TKE (Vtke), the cross-axis part of the roll TKE, or the horizontal parts of the nonlineal TKE.

In Glendening's lineal TKE budget of a boundary layer during a mature-roll stage, the net nonlinear interaction was negative in the lower boundary layer and positive in the upper boundary layer, in qualitative agreement with our results for a roll updraft stage presented in Fig. 7 (which necessarily shows only the cloudy upper boundary layer). The stress work and roll vertical velocity shear stress had opposite signs, with the shear stress being positive in the lower boundary layer and negative in the upper boundary layer. LeMone (1976) reported positive roll vertical velocity shear stress in the lower boundary layer, calculated from aircraft data, also in agreement with the results of Glendening. Glendening evaluated the roll-scale TKE budget at a mature-roll stage, acknowledging that the budget may be different at other stages in the roll life cycle. The stress work and roll shear stress terms for downdraft stages (not shown) have the opposite signs compared to those in roll updraft stages.

Vertical profiles of the net nonlinear interaction, normalized by w_*^3/z_i, are shown as a function of stage in Fig. 8. The sign of the net nonlinear interaction is generally positive for the roll updraft stages, representing a source term for the roll-scale TKE. This pattern is consistent with Glendening's assertion, supported by the results of Khanna and Brasseur (1998), that the upscale energy transfer occurs primarily in the roll updraft regions as individual plumes merge into lineal roll motion. Conversely, during the downdraft stages, the nonlinear interaction term is generally negative, representing downscale energy transfer. Glendening's profile of the nonlinear interaction term for the mature-roll case is negative in the lower boundary layer and positive in the upper boundary layer, peaking around 0.8 z_i. While the trends in the sign of the profiles are consistent with Glendening, the profiles presented here do not, in gen-

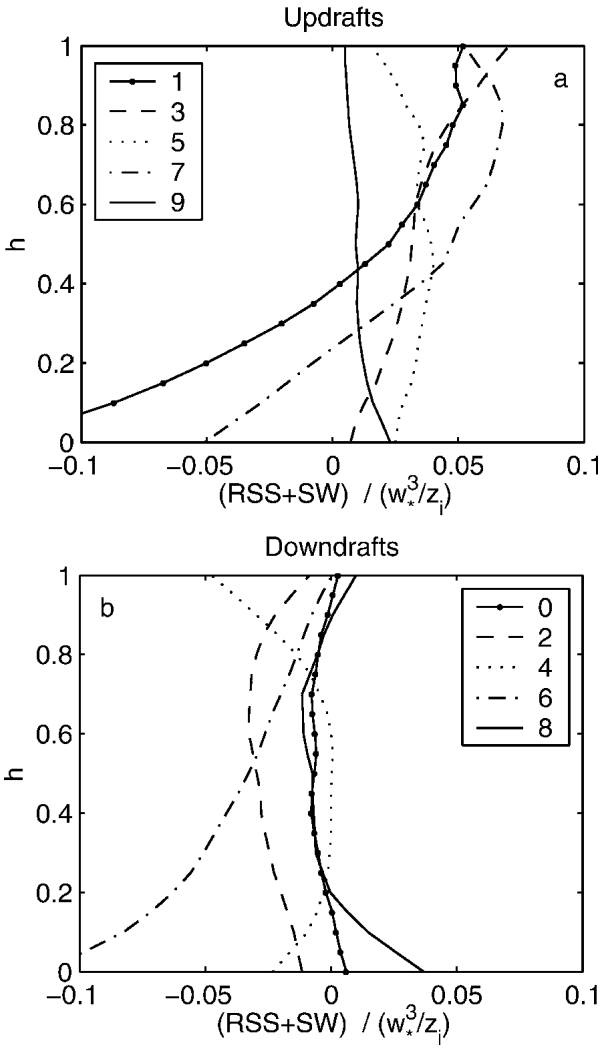

FIG. 8. Composited vertical profiles of net nonlinear interaction (i.e., the sum of stress work and vertical roll shear stress), normalized by w_*^3/z_i, for (a) roll updraft stages and (b) roll downdraft stages. The cloud normalized height h is defined to be zero at cloud base and one at cloud top. The numbers in the legend indicate the stages.

eral, tend to zero near cloud top; this difference may be due to retrieval problems near cloud top or statistical limitations.

We integrate the sum of the two dominant roll-turbulence nonlinear interaction terms over the cloud layer to determine the net effect of the interactions (Fig. 9). Nonlinear interactions between the roll and turbulence scales are a source to roll-scale TKE primarily during stages 3, 5, and 7, roughly coinciding with the maximum of the roll-scale variance during stages 2–7 (Fig. 5), rather than coinciding with the large increase in roll-scale TKE that occurs during stages 0–2. During stages 0 and 9 both the roll shear stress and the stress work are nearly zero (Fig. 6). During stages 1, 4, and 8, the two terms nearly balance each other, and the net value is small. The net nonlinear interaction is a sink to the roll-scale TKE during stages 2 and 6. As in Fig. 8, the roll updraft and roll downdraft pattern is consistently apparent in Fig. 9a. Averaging over successive downdraft and updraft stages together, rather than each stage individually, yields qualitatively similar results (Fig. 9b) without the updraft and downdraft pattern of Fig. 9a. The error bars indicate that the net nonlinear interaction during stages 0–1 are likely negative, and thus a sink to the roll-scale TKE. Similarly, during stages 4–5, the net nonlinear interaction is positive, and thus a source to the roll-scale TKE.

We can relate the shapes of the profiles (Fig. 8) and the signs of the integrated values (Fig. 9a) to the trends in the turbulence-scale vertical velocity variance profiles (Fig. 2), using the expression

$$\mathrm{SW} + \mathrm{RSS} = -\frac{\partial(\overline{w^r w^t w^t})}{\partial z} + \overline{w^t w^t \frac{\partial w^r}{\partial z}} = \overline{-w^r \frac{\partial w^t w^t}{\partial z}}$$

$$\simeq -\overline{w^r}\,\overline{\frac{\partial w^t w^t}{\partial z}}, \qquad (3)$$

noting that the last step is only strictly true for constant w^r over the averaging interval. (We assume constant w^r for the purpose of the following discussion only; it is not necessary to make such an assumption for our calculations.) For example, the turbulence-scale vertical velocity variance profiles during stage 1 are characterized by in-cloud maxima (Figs. 2 and 3), with positive slopes in the lower half of the cloud layer and negative slopes in the upper half. Since stage 1 is a roll updraft stage ($\overline{w^r} > 0$), the net nonlinear interaction is negative in the lower half of the cloud layer and positive in the upper half (Fig. 8a). The integrated value is thus nearly zero (Fig. 9). In contrast, stage 3 does not have persistent in-cloud turbulence-scale vertical velocity variance maxima (Figs. 2 and 3). Instead the turbulence-scale variance generally decreases with height or has little dependence on height. When the turbulence-scale variance decreases linearly with height, the slope is negative; thus the net nonlinear interaction is positive throughout the entire cloud layer if $\overline{w^r} > 0$ is positive, as it is for stage 3 (Fig. 8a). The integrated

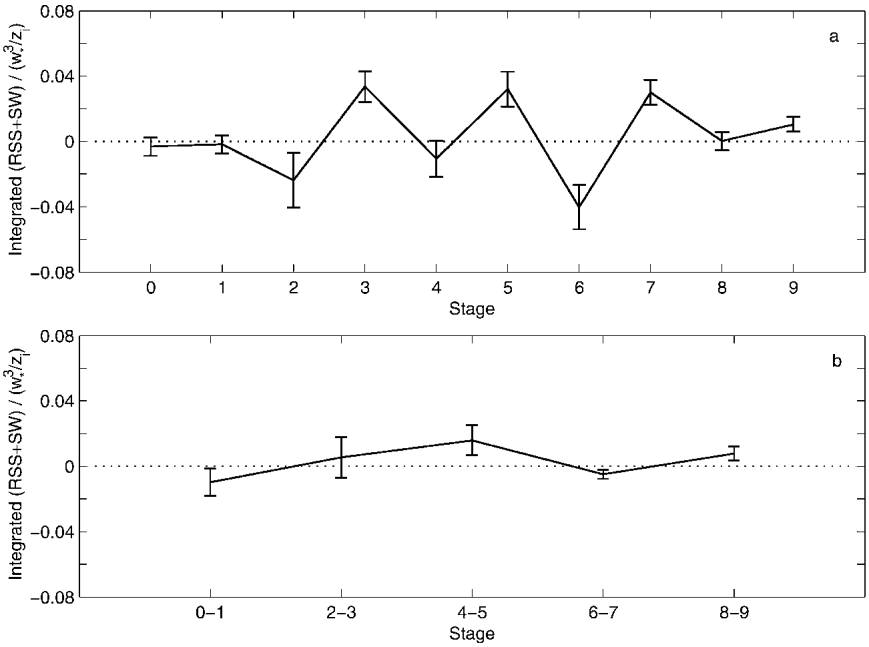

FIG. 9. (a) Composite of the net nonlinear interaction (i.e., the sum of stress work and roll shear stress), normalized and integrated over the cloud layer, as a function of stage in the roll life cycle. Error bars indicate the standard deviation of the mean of the three composited cycles. (b) Same as (a), except that stages 0–1, 2–3, 4–5, 6–7, and 8–9 are grouped together.

net nonlinear interaction is then positive for stage 3 (Fig. 9).

All of the turbulence transport terms, including stress work but not roll shear stress, must individually sum to zero over the depth of the boundary layer, assuming no transport to the free atmosphere. When the stress work term, integrated over the cloud layer, is positive, it must be negative below cloud. While stress work acts to strengthen the rolls in the cloud layer [where we observe the changes in roll organization with cloud radar and Weather Surveillance Radar-1988 Doppler (WSR-88D)], the roll motion must be correspondingly less organized in the subcloud layer.

The liquid water content variations in a cloud are typically closely related to the variation of vertical velocity (Fig. 2-16 of Pruppacher and Klett 1997; Chlond 1992), which is caused primarily by buoyancy. The composite of the mean value (rather than the variance) of the unfiltered vertical velocity, integrated through the depth of the cloud, is shown as a function of stage in Fig. 10a. The roll updraft (odd-numbered stages) and downdraft (even-numbered stages) structure is readily apparent. The maximum in the mean vertical velocity occurs during stage 1. We can thus infer that more condensation of liquid and deposition of ice occurred during stage 1 than any other stage. The associated latent heating contributes to in-cloud buoyancy, which in turn produces primarily turbulence-scale TKE. In addition to the primary peak at stage 1, there is a secondary peak of mean vertical velocity at stage 7. The composite of the unfiltered mean vertical velocity is also shown in Fig. 10b, in which successive downdrafts and updrafts are grouped together. The mean vertical velocity is relatively low during stages 2–5.

b. *Conceptual model for the role of scale interactions*

While we cannot address with certainty the direct role of scale interactions in the initiation of the observed transient linear organization, there are intriguing patterns, summarized in Fig. 11. The largest change in the roll TKE observed with the cloud radar (2×10^{-5} m^2 s^{-3}) occurs between stages 0 and 1. The roll-scale TKE also increases between stages 1 and 2. During stage 1, the large mean vertical velocity (Fig. 10; induced from the surface buoyancy) probably leads to increased condensation and deposition, and subsequent latent heating and in-cloud buoyancy. This is a possible explanation for the secondary maximum in the turbulence-scale vertical velocity variance at stage 1 (Figs. 2 and 3). The corresponding idealized turbulence-scale variance profile is shown in Fig. 11, including the secondary maximum, as well as a subcloud turbulence-scale variance peak (which presumably is present throughout the analysis period). The consistent turbulence-scale variance peak during roll strengthening suggests that the rolls extract energy from the turbulence scale, although the method is not clear from this study.

The roll-scale TKE is fairly steady from stages 3 through 5. The idealized roll-scale variance profile de-

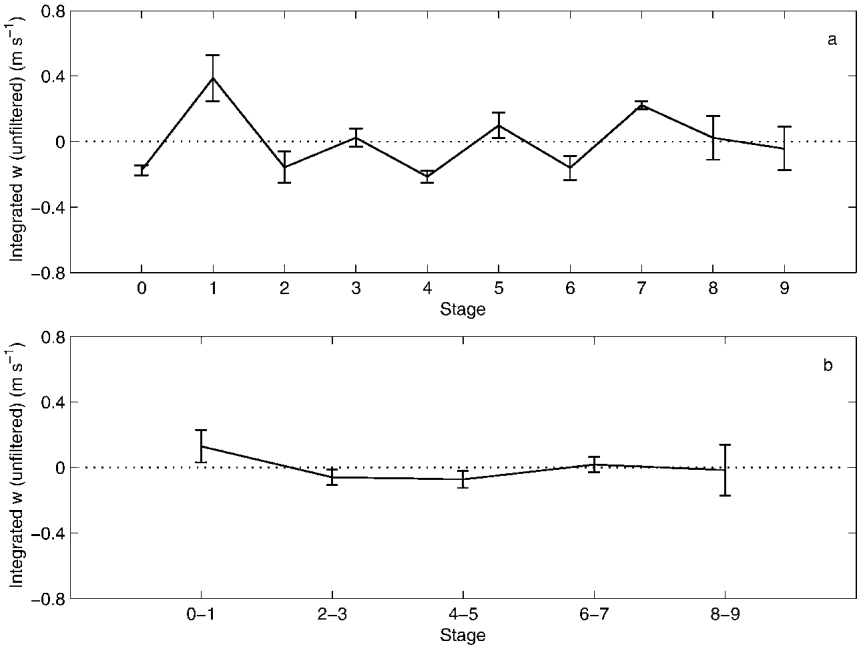

FIG. 10. (a) Composite of unfiltered mean vertical velocity averaged over the cloud depth, as a function of stage in the roll life cycle. (b) Same as (a), except stages 0–1, 2–3, 4–5, 6–7, and 8–9 are grouped together.

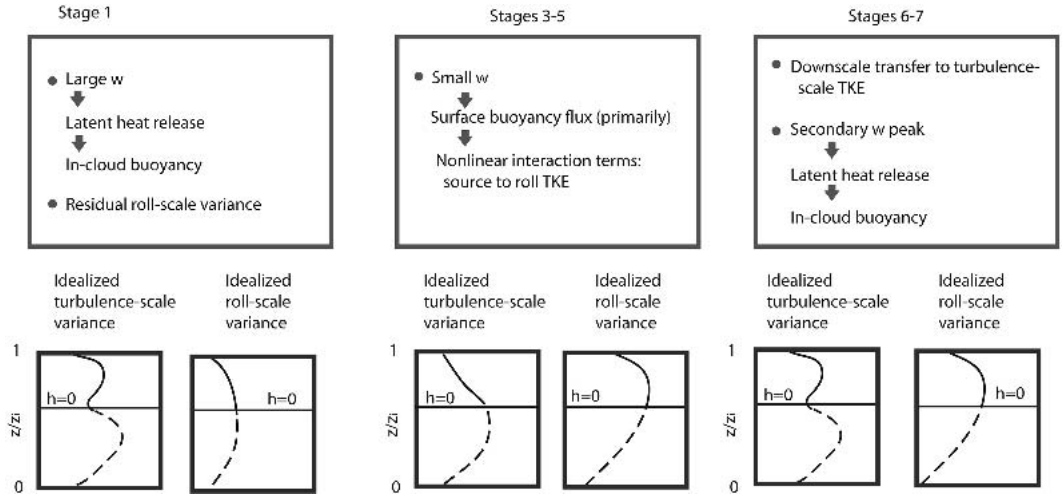

FIG. 11. Summary of contributors to the roll life cycle. Solid lines indicate idealized vertical velocity variance profiles observed in this study, while dashed lines indicate a "best guess" of the vertical velocity variance profiles below cloud base.

picted in Fig. 11 shows large roll-scale variance in the cloud layer and less in the subcloud layer. During the roll updraft stages 3 and 5, the mean vertical velocity is smaller than the other updraft stages (Fig. 10), and the in-cloud turbulence-scale variance peak is consequently absent. The variance depicted in the idealized profile is primarily due to the surface buoyancy flux. Thus the turbulence-scale vertical velocity variance decreases with height within the cloud—allowing the integrated nonlinear interaction term to be a significant source to the in-cloud roll-scale TKE. The net nonlinear interaction is a source to the rolls in the middle stage of the roll life cycle. We thus have localized—in space and time—upscale TKE transfer. The magnitude of the net nonlinear interaction is significant in stages 4–5 (6×10^{-5} m^2 s^{-3}). This magnitude is roughly 3 times that of the change in roll-scale TKE observed between stages 0 and 1, but does not coincide with the change in roll-scale TKE. It seems likely that there is a sink to the roll-scale TKE that balances the nonlinear interaction source, leading to fairly steady roll-scale TKE during the middle stages.

From stages 7 through 9, the roll-scale TKE decreases slowly. During stage 6, the net nonlinear interaction is a sink for the roll-scale TKE. During stage 7, the mean vertical velocity is about midway between that of stages 1 and 5 (Fig. 10). The observed in-cloud turbulence-scale vertical velocity variance peaks (Fig. 2) and the positive turbulence-scale peakedness parameter (Fig. 3) for stages 7–8 indicates that the slight increase in mean vertical velocity may have caused additional latent heating. The net contribution from nonlinear interactions from stages 6 and 7 taken together is a small sink to the roll-scale TKE. The roll-scale variance decreases during the later stages, but a small residual remains, allowing the next cycle to begin.

c. Eulerian versus Lagrangian description

Although we have focused on a Eulerian description in our discussion of the nonlinear interactions, a Lagrangian perspective may be necessary to fully understand the phenomenon. Changes in organization and variance profiles may not be caused locally, instead being delayed by the advection time from the source region. In the satellite image (1943 UTC; Fig. 1 in Part I), the convective organization appears to change with fetch across the lake. Near the upwind shore, there are hints of linear organization visible in the clouds. The organization is mostly cellular over the middle of the lake and linear near the downwind shore. Although there are no data available across the southern part of Lake Michigan, we use surface measurements for the upwind (Sheboygan) and downwind (Montague) ISS sites to estimate the change in u_*/w_* across the lake. We assume that values measured at 1943 UTC at the two ISS sites are representative of the temperature difference between the lake surface and the air, and that the wind speed varies linearly with fetch across the lake. We further assume the depth of the boundary layer varies as $z_i = a\sqrt{x} + b$, where x is fetch, and a and b are constants (Chang and Braham 1991). We use z_i = 340 m for the upwind shore and z_i = 890 m for the downwind shore. The resulting schematic diagram of u_*/w_* across the lake is shown in Fig. 12. The combination of increasing boundary layer depth, increasing wind speed, and decreasing temperature difference across the lake leads to more favorable conditions for rolls (at least in regard to the value of u_*/w_*) near the upwind shore, less favorable conditions over the middle of the lake, and recovering u_*/w_* by the downwind shore. The roll decay time, estimated as the convective time scale z_i/w_*, is about 10 min, much less than the 4-h

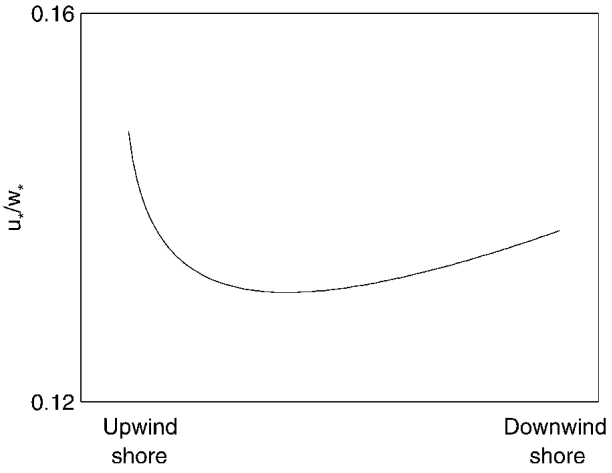

FIG. 12. Schematic diagram of u_*/w_* from the upwind shore to the downwind shore.

advection time across the lake. Thus the convective organization should reflect the spatial changes in atmospheric conditions. The trend in Fig. 12 is consistent with the organization in the satellite picture shown in Fig. 1 of Part I. Over the land, where there is linear organization, the temperature difference between the surface and the air is (presumably) decreased, and thus the total heat flux is decreased and u_*/w_* is increased.

4. Discussion

We suggest that nonlinear scale interactions are significant and may contribute in some way to the convective organization switching to rolls even though the atmospheric conditions are not favorable. The two significant nonlinear interaction terms are vertical transport of turbulence-scale TKE by the rolls (stress work) and roll shear stress interscale transfer.

In general, interscale transfer is globally downscale, that is, from large scales to small scales. In the convective boundary layer, the production terms in the total TKE equation, mean shear and buoyancy, add TKE to the large-scale, energy-containing eddies. In a process called the energy cascade, this energy is transferred through the inertial subrange to the smallest eddies where it undergoes viscous dissipation. Although the net transfer is downscale, there may be occasional, local transfers of energy upscale, from subgrid to resolved scales, called "backscatter" (Mason and Thompson 1992; Tong et al. 1999). However, backscatter typically refers to exchanges between the subgrid scales and resolved, energy-containing scales, whereas the present work (and also Glendening) discusses the exchange of energy between two different scales, both in the energy-containing range. In our case the only true interscale transfer term is the roll shear stress, but stress work is locally a source to roll-scale TKE from turbulence-scale TKE as well.

During a mature-roll stage (stage 5), the stress work term is positive, the roll shear stress term is negative, and their sum is positive, in the upper part of the boundary layer (Fig. 7). These results are consistent with the mature-roll observations in the lower boundary layer by LeMone (1976) and the LES results of Glendening. The signs of the various terms change with stage in the roll life cycle.

The magnitudes of the maxima of the net nonlinear interaction (Figs. 8a and 8b) are much less than the maximum magnitude given by Glendening. There are several factors contributing to this apparent discrepancy. The magnitudes of the nonlinear interaction terms depend to a certain extent on the width of the bandpass filters applied to the data. This problem is not an issue for Glendening because his analysis is in physical space rather than frequency space. Second, differing atmospheric conditions between Glendening's LES results and the present results also complicate the comparison. The case modeled by Glendening was strongly sheared ($u_* = 0.48$ m s^{-1}) and weakly convective ($w_* = 0.89$ m s^{-1}), whereas the present case had weaker shear ($u_* = 0.20$ m s^{-1}) and stronger convection ($w_* = 1.55$ m s^{-1}). Although the results are normalized by using w_*, it is unlikely that w_* is the only scaling parameter since there are many other processes, such as shear, longwave and shortwave radiation, latent heating, surface fluxes, and entrainment, that are important in cloudy boundary layers (Nicholls 1989; Duynkerke et al. 1995).

Composites of vertically integrated (through the cloud layer) net nonlinear interaction (Fig. 8c) are consistent with upscale energy transfer primarily in roll updraft regions, as individual plumes merge into lineal roll motion. Glendening also found net upscale energy transfer in the upper boundary layer in his analysis of a mature roll. LeMone (1976) calculated the energy exchange between roll and turbulence scales and found the energy exchange term to be considerably smaller than the largest source of roll-scale TKE buoyancy. In Glendening's roll-scale vertical TKE budget, the upscale energy transfer in the upper part of the boundary layer is about one-third the magnitude of the buoyancy production term peak in the middle part of the boundary layer.

In explaining changes in the observed variance profiles, latent heating plays an integral role. Hjelmfelt (1990) found latent heating to amplify lake-effect mesoscale circulations. Olsson and Harrington (2000) found latent heating to contribute substantially to the TKE, which is also suggested by the present results. More directly relevant to the present work are the results of Rao and Agee (1996), who showed that latent heating increased the vertical velocity variance in the upper part of the cloud. In the present study, decreased latent heating in the middle stages of the roll life cycle leads to strengthening of nonlinear interactions. Whereas Chlond (1992) and Cooper et al. (2000)

found that latent heating intensified rolls, Brümmer (1997, 1999) found latent heating to be more important in the generation of cellular convection, in general agreement with the present results. Brasseur and Wei (1994) suggested that energy may move upscale from energy-containing scales (the turbulence scale in our case) to larger scales (the roll scale in our case) when there temporarily is no production of TKE.

There are several issues regarding the interscale transfer and turbulent transport terms that we cannot address in the present work: 1) the horizontal roll shear stress term in the roll-scale vertical TKE equation, 2) the nonlinear interaction and turbulent transport terms in the roll-scale horizontal TKE equation, and 3) the turbulent transport and nonlinear interaction terms in either equation in the subcloud layer. The first point may not be problematic because Glendening found $\overline{u^t w^t}\,\partial\overline{w^r}/\partial z$, that is, the roll shear stress term, to be much smaller than the other two nonlinear interaction terms ($-\partial\overline{w^r}\,\overline{w^t w^t}/\partial z$ and $\overline{w^t w^t}\,\partial\overline{w^r}/\partial z$). The budget of the roll-scale horizontal TKE, however, is potentially important, since roll-scale vertical TKE is converted to roll-scale horizontal TKE through the pressure term. For the roll-scale horizontal TKE budget presented by Glendening, the nonlinear interaction terms are a large sink in the lower half of the boundary layer. The pressure term is a large source to roll-scale horizontal TKE in the lower half of the boundary layer, a smaller source in the upper boundary layer, and a small sink above z_i. The shear contributes relatively little to roll-scale horizontal TKE, with only a small source above z_i. Glendening's results indicate that buoyancy is the most important production term for roll-scale TKE, not shear; his results suggest roll-scale vertical TKE is more important to mode switching than roll-scale horizontal TKE. The third point is crucial. Vertical transport terms, including the stress work term, must integrate to zero over the entire boundary layer. The stress work term is the largest of the nonlinear interaction terms, and consequently the strengthening of the rolls in the cloud layer must be associated with compensating weakening of the rolls in the subcloud layer. The rolls may thus become detached from the surface. It is only the linear organization in the cloud layer that we seek to explain since both the WSR-88D and cloud radar measurements are in-cloud.

While our dataset is limited, we have shown that nonlinear scale interactions may be important in this marginal case. There are consistent in-cloud turbulence-scale vertical velocity variance peaks both before and after the maximum in roll intensity. We have shown how changes in latent heating are related to nonlinear-scale interactions and the roll-scale TKE budget. Nonlinear-scale interactions, while difficult to measure, may help explain observations of rolls that occur in unlikely conditions.

5. Conclusions

Cloud radar vertical velocity data, collected on 13–14 January 1998 during the Lake-Induced Convection Experiment, reveal transient linear organization. The duration of the radar measurements is nearly 18 h, encompassing three cycles of marginally linearly organized convection switching to more unorganized cellular convection and back again. In the companion paper (Part I) we have shown that this lake-effect event, with large positive buoyancy flux and only moderate shear, was not within the range of buoyancy parameters most often associated with rolls. No correlation of atmospheric conditions (boundary layer mean shear, low-level shear, shear curvature, temperature, buoyancy flux, and stability parameter) was found with the observed organization.

While we cannot address with certainty the direct role of scale interactions in the initiation of the observed transient linear organization, there are intriguing patterns in the variance profiles. The mean vertical velocity was highest during roll strengthening and had a smaller maximum during roll decay. Since mean vertical velocity is typically found to be correlated with liquid water content, the increase may be associated with additional latent heating, providing turbulent kinetic energy (TKE) to the turbulence-scale eddies. In agreement with this scenario, we observed in-cloud turbulence-scale vertical velocity variance peaks during both roll strengthening and roll decay.

The two dominant nonlinear interaction terms for the roll-scale TKE are the vertical transport of turbulence-scale TKE by the rolls (stress work) and roll shear stress interscale transfer. Since the sum of these terms is proportional to the gradient of the turbulence-scale variance, the in-cloud net nonlinear interaction is minimized when an in-cloud turbulence-scale vertical velocity variance peak is observed and maximized when the in-cloud turbulence-scale vertical velocity variance decreases with height. Consequently nonlinear interaction is a source to the rolls in the middle stages of the roll life cycle observed in this case. Net nonlinear interaction between the roll scales and the turbulence scales was observed and found to be significant in magnitude.

While there are important questions that cannot be answered with this dataset, we suggest that nonlinear-scale interactions are significant and may contribute in some way to the convective organization switching to rolls even though the atmospheric conditions are not necessarily good for rolls. Within the limitations of this study, nonlinear interactions appear to play some role in transitions in mesoscale organization and thus warrant further study. An LES study of the role of nonlinear interactions in causing transitions in mesoscale organization would be particularly useful.

The processes by which heat and moisture are transferred from warm water surfaces to the comparatively

cold atmosphere occur over a wide range of spatial scales. Roll-scale circulations significantly modify the environment of the smaller-scale turbulence phenomena. Likewise, turbulence-scale eddies are the intermediate agents between the enhanced surface fluxes and the intensification of the roll-scale circulations. Much is still not understood about these important processes, and still less is known about interactions between processes on each of these scales. An understanding of how these processes work in conjunction to link the surface to roll-scale flows is necessary if we are to develop more accurate models of large-scale storm development.

Acknowledgments. We would like to acknowledge George Young, John Wyngaard, Jerry Harrington, Eugene Clothiaux, David Babb, Charles Pavloski, Laura Hinkelman, and Dave Kristovich for many helpful discussions. The ISS data were obtained from E. Miller (NCAR/ATD). Lake surface temperatures were provided by the Great Lakes Environmental Research Laboratory (GLERL) Coastwatch program. The PSU radar was hosted in Muskegon by the GLERL Lake Michigan Field Station. Wavelet analysis software was provided by C. Torrence and G. Compo and is available at http://paos.colorado.edu/research/wavelets/. This work was supported by the National Science Foundation under Grants ATM-9596107, ATM-9629343, ATM-0127360, and ATM-9873643.

REFERENCES

Atlas, D., B. Walter, S.-H. Chou, and P. J. Sheu, 1986: The structure of the unstable marine boundary layer viewed by lidar and aircraft observations. *J. Atmos. Sci.,* **43,** 1301–1318.

Braham, R. R., Jr., 1986: Cloud and motion fields in open cell convection over Lake Michigan. Preprints, *23d Conf. on Radar Meteorology and Conf. on Cloud Physics,* Snowmass, CO, Amer. Meteor. Soc., JP202–JP205.

Brasseur, J. G., and C.-H. Wei, 1994: Interscale dynamics and local isotropy in high Reynolds number turbulence within triadic interactions. *Phys. Fluids,* **6,** 842–870.

Brümmer, B., 1985: Structure, dynamics, and energetics of boundary layer rolls from KonTur aircraft observations. *Beitr. Phys. Atmos.,* **58,** 237–254.

——, 1997: Boundary layer mass, water, and heat budgets in wintertime cold-air outbreaks from the Arctic sea ice. *Mon. Wea. Rev.,* **125,** 1824–1837.

——, 1999: Roll and cell convection in wintertime Arctic cold-air outbreaks. *J. Atmos. Sci.,* **56,** 2613–2636.

Chang, H.-R., and H. N. Shirer, 1984: Transitions in shallow convection: An explanation for lateral cell expansion. *J. Atmos. Sci.,* **41,** 2334–2346.

Chang, S. S., and R. R. Braham Jr., 1991: Observational study of a convective internal boundary layer over Lake Michigan. *J. Atmos. Sci.,* **48,** 2265–2279.

Chlond, A., 1992: Three-dimensional simulation of cloud street development during a cold air outbreak. *Bound.-Layer Meteor.,* **58,** 161–200.

Cooper, K. A., M. R. Hjelmfelt, R. G. Derickson, D. A. R. Kristovich, and N. F. Laird, 2000: Numerical simulation of transitions in boundary layer convective structures in a lake-effect snow event. *Mon. Wea. Rev.,* **128,** 3283–3295.

Deardorff, J. W., 1980: Stratocumulus-capped mixed layers derived from a three-dimensional model. *Bound.-Layer Meteor.,* **18,** 495–527.

Duynkerke, P. G., H. Q. Zhang, and P. J. Jonker, 1995: Microphysical and turbulent structure of nocturnal stratocumulus as observed during ASTEX. *J. Atmos. Sci.,* **52,** 2763–2777.

Frisch, A. S., D. H. Lenschow, C. W. Fairall, W. H. Schubert, and J. S. Gibson, 1995: Doppler radar measurements of turbulence in marine stratiform cloud during ASTEX. *J. Atmos. Sci.,* **52,** 2800–2808.

Glendening, J. W., 1996: Lineal eddy features under strong shear conditions. *J. Atmos. Sci.,* **53,** 3430–3448.

——, 2000: Budgets of lineal and nonlineal turbulent kinetic energy under strong shear conditions. *J. Atmos. Sci.,* **57,** 2297–2318.

Harrington, J. Y., and P. Q. Olsson, 2001: On the potential influence of ice nuclei on surface-forced marine stratocumulus cloud dynamics. *J. Geophys. Res.,* **106** (D21), 473–484.

Hartmann, J., C. Kottmeier, and S. Raasch, 1997: Roll vortices and boundary-layer development during a cold air outbreak. *Bound.-Layer Meteor.,* **84,** 45–65.

Hein, P. F., and R. A. Brown, 1988: Observations of longitudinal roll vortices during Arctic cold air outbreaks over open water. *Bound.-Layer Meteor.,* **45,** 177–199.

Hildebrand, P. H., and B. Ackerman, 1984: Urban effects on the convective boundary layer. *J. Atmos. Sci.,* **41,** 76–91.

Hjelmfelt, M. R., 1990: Numerical study of the influence of environmental conditions on lake-effect snowstorms over Lake Michigan. *Mon. Wea. Rev.,* **118,** 138–150.

Khanna, S., and J. G. Brasseur, 1998: Three-dimensional buoyancy- and shear-induced local structure of the atmospheric boundary layer. *J. Atmos. Sci.,* **55,** 710–743.

Kristovich, D. A. R., N. F. Laird, M. R. Hjelmfelt, R. G. Derickson, and K. A. Cooper, 1999: Transitions in boundary layer meso-γ convective structures: An observational case study. *Mon. Wea. Rev.,* **127,** 2895–2909.

Lappen, C.-L., and D. A. Randall, 2001: Toward a unified parameterization of the boundary layer and moist convection. Part III: Simulations of clear and cloudy convection. *J. Atmos. Sci.,* **58,** 2052–2072.

LeMone, M. A., 1973: The structure and dynamics of horizontal roll vortices in the planetary boundary layer. *J. Atmos. Sci.,* **30,** 1077–1091.

——, 1976: Modulation of turbulence energy by longitudinal rolls in an unstable planetary boundary layer. *J. Atmos. Sci.,* **33,** 1308–1320.

——, and W. T. Pennell, 1976: The relationship of trade wind cumulus distribution to subcloud layer fluxes and structure. *Mon. Wea. Rev.,* **104,** 524–539.

Lenschow, D. H., and B. B. Stankov, 1986: Length scales in the convective boundary layer. *J. Atmos. Sci.,* **43,** 1198–1209.

Mason, P. J., and D. J. Thompson, 1992: Stochastic backscatter in large-eddy simulations of boundary layers. *J. Fluid Mech.,* **242,** 51–78.

Melfi, S. H., J. D. Spinhirne, S.-H. Chou, and S. P. Palm, 1985: Lidar observations of vertically organized convection in the planetary boundary layer over the ocean. *J. Climate Appl. Meteor.,* **24,** 806–821.

Miles, N. L., and J. Verlinde, 2005: Observations of transient linear organization and nonlinear scale interactions in lake-effect clouds. Part I: Transient linear organization. *Mon. Wea. Rev.,* **133,** 677–691.

Moeng, C.-H., 1984: A large-eddy-simulation model for the study of planetary boundary-layer turbulence. *J. Atmos. Sci.,* **41,** 2052–2062.

Mourad, P. D., and R. A. Brown, 1990: Multiscale large eddy stages in weakly stratified planetary boundary layers. *J. Atmos. Sci.,* **47,** 414–438.

Moyer, K. A., and G. S. Young, 1994: Observations of mesoscale cellular convection from the marine stratocumulus phase of FIRE. *Bound.-Layer Meteor.,* **71,** 109–133.

Müller, G., and A. Chlond, 1996: Three-dimensional numerical study of cell broadening during cold-air outbreaks. *Bound.-Layer Meteor.,* **81,** 289–323.

Nicholls, S., 1978: Measurements of turbulence by an instrumented aircraft in a convective atmospheric boundary layer over the sea. *Quart. J. Roy. Meteor. Soc.,* **104,** 653–676.

——, 1984: The dynamics of stratocumulus: Aircraft observations and comparisons with a mixed layer model. *Quart. J. Roy. Meteor. Soc.,* **110,** 783–820.

——, 1989: The structure of radiatively driven convection in stratocumulus. *Quart. J. Roy. Meteor. Soc.,* **115,** 487–511.

Olsson, P. Q., and J. Y. Harrington, 2000: Dynamics and energetics of the cloudy boundary layer in simulations of off-ice flow in the marginal ice zone. *J. Geophys. Res.,* **105** (D9), 889–899.

Pruppacher, H. R., and J. D. Klett, 1997: *Microphysics of Clouds and Precipitation.* 2d ed. Kluwer Academic, 954 pp.

Rabin, R. M., R. J. Doviak, and A. Sundara-Rajan, 1982: Doppler radar observations of momentum flux in a cloudless convective layer with rolls. *J. Atmos. Sci.,* **39,** 851–863.

Rao, G.-S., and E. M. Agee, 1996: Large eddy simulation of turbulent flow in a marine convective boundary layer with snow. *J. Atmos. Sci.,* **53,** 86–100.

Reinking, R. F., R. J. Doviak, and R. O. Gilmer, 1981: Clear-air roll vortices and turbulent motions as detected with an airborne gust probe and dual-Doppler radar. *J. Appl. Meteor.,* **20,** 678–685.

Rothermel, J., and E. M. Agee, 1986: A numerical study of atmospheric convective scaling. *J. Atmos. Sci.,* **43,** 1186–1197.

Sommeria, G., and M. A. LeMone, 1978: Direct testing of a three-dimensional model of the planetary boundary layer against experimental data. *J. Atmos. Sci.,* **35,** 25–39.

Sykes, R. I., and D. S. Henn, 1988: On the numerical computation of two-dimensional convective flow. *J. Atmos. Sci.,* **45,** 1961–1964.

——, W. S. Lewellen, and D. S. Henn, 1988: A numerical study of the development of cloud-street spacing. *J. Atmos. Sci.,* **45,** 2556–2569.

Tong, C., J. C. Wyngaard, and J. G. Brasseur, 1999: Experimental study of the subgrid-scale stresses in the atmospheric surface layer. *J. Atmos. Sci.,* **56,** 2277–2292.

Weckwerth, T. M., T. W. Horst, and J. W. Wilson, 1999: An observational study of the evolution of horizontal convective rolls. *Mon. Wea. Rev.,* **127,** 2160–2179.

Wyngaard, J. C., 2002: On the rate of energy transfer in isotropic turbulence. *Phys. Fluids,* **14,** 2426–2431.

Young, G. S., 1988: Turbulence structure of the convective boundary layer. Part I: Variability of normalized turbulence statistics. *J. Atmos. Sci.,* **45,** 719–726.

——, B. K. Cameron, and E. E. Hebble, 2000: Observations of the entrainment zone in a rapidly entraining boundary layer. *J. Atmos. Sci.,* **57,** 3145–3160.